CHAPTER 8

On the role of resource complementarity in siting renewable power plants and its impact on power system design and economics

Mathias Berger, David Radu and Damien Ernst
Department of Electrical Engineering and Computer Science, University of Liège, Belgium

8.1 Introduction

Wide-ranging electrification and the large-scale deployment of technologies harnessing renewable resources for electricity production have long been viewed as a means of achieving deep decarbonization targets. However, widely-available renewable resources such as solar irradiance and wind are inherently variable on time scales ranging from minutes to years (Engeland et al., 2017), which complicates power system planning and operation procedures, especially in systems with inflexible electricity loads.

Since the distribution of variable renewable energy resources is heterogeneous in space and time, several authors suggested that carefully selecting renewable power generation sites to take advantage of this diversity could at least partly alleviate variability issues and reduce the residual load (Giebel, 2000; Milligan and Artig, 1999). The concept of complementarity of (and between) renewable resources, which captures this intuition, has received much attention of late and a number of metrics have been proposed to measure it (Jurasz et al., 2020). Moreover, recent improvements in meteorological modeling and observation instruments have unlocked vast amounts of high-resolution climatological data that can be readily leveraged in the context of asset siting analyses (e.g., reanalysis datasets providing hourly-sampled solar irradiance and wind speed data for thousands of candidate sites over several decades), as mathematical programming techniques are particularly well-suited for exploiting such data and systematically identifying sets of locations whose renewable resources exhibit some degree of complementarity.

Nevertheless, to the authors' best knowledge, only a handful of papers have sought to take advantage of such datasets and methods in order to carry out large-scale, highly-granular asset siting analyses (i.e., comprising more than a few dozen candidate sites).

Complementarity of Variable Renewable Energy Sources.
DOI: https://doi.org/10.1016/B978-0-323-85527-3.00021-2

In particular, Musselman et al. (2018) proposed two mixed-integer linear programming models that seek to site wind power plants so as to balance two competing objectives, namely simultaneously minimizing the average residual demand and either the average step-wise power output variability or the maximum increase in residual demand over time intervals of prespecified length. Similarly, Wu et al. (2017) appear to use a linear programming model[1] that sites and sizes wind power plants so as to minimize the maximum residual demand. Finally, Berger et al. (2021) proposed combinatorial optimization models that site renewable power plants so as to minimize the empirical probability that most sites simultaneously experience low electricity production levels relative to a prespecified fraction of the electricity demand.

Furthermore, the benefits of renewable resource complementarity are often evaluated for small sets of power plants or at system-level using non-monetary metrics such as the residual electricity demand (Musselman et al., 2018; Wu et al., 2017) and models of the underlying power system are rarely considered. Hence, these approaches typically fail to properly assess the implications that complementarity may have for power system design and economics, which necessitates the use of detailed integrated capacity expansion planning (CEP) models. Indeed, such models represent the planning and operation of power systems in a temporally and spatially-resolved fashion, which makes it possible to properly account for the interaction between different technologies (e.g., generation, transmission, and storage) as well as system-level effects such as network congestion.

This chapter analyses the role that complementarity may play in renewable power generation asset siting decisions and its impact on power system design and economics. To this end, a two-stage approach is employed (Radu et al., 2022). In the first stage, a siting method is used to select a prespecified number of sites optimizing a predefined siting criterion. In the second stage, the set of sites identified in the first stage is passed to a joint generation-transmission-storage CEP model, which then identifies the optimal power system configuration. Seven different siting schemes adapted from the literature are analyzed in a case study focusing on the deployment of onshore wind power plants in the European power system. In the interest of transparency and in order to spur the adoption of such workflows by other researchers, the models, computer code, and data used in this chapter are all made available to the community (Dubois et al., 2021; Radu et al., 2021).

8.2 Methodology

This section describes the two-stage approach used to assess the impact of resource complementarity on renewable power plant siting decisions and its implications for power

[1] The exact nature of the model used is unclear. The authors mention a "linear optimization model" in the main document (where no formulation is provided) and an "integer optimization model" in the supplementary material (where the formulation is shown but few explanations are offered).

system design and economics. Some notation is first introduced. Then, the siting and CEP frameworks are discussed.

8.2.1 Preliminaries

Space and time: A finite time horizon $T \in \mathbb{N}$ and associated set of time periods $\mathcal{T} = \{1, \ldots, T\}$ are considered. A geographical region is represented by a finite set of locations $\mathcal{L}, |\mathcal{L}| = L$, where renewable power generation assets may be deployed.

Renewable sites: Each location $l \in \mathcal{L}$ is assumed to have a fixed technical potential $\bar{\kappa}_l \in R_+$, which represents the power generation capacity that may be deployed at this location. In addition, a time series $\mathbf{s}_l = (s_{l1}, \ldots, s_{lT})^\top \in \mathbb{R}_+^T$ of renewable resource data (e.g., wind speed, solar irradiation) is assumed to be available at each site $l \in \mathcal{L}$. The normalized instantaneous power output of location $l \in \mathcal{L}$ is estimated via a suitable transfer function h_l providing per-unit capacity factor values $\pi_{lt} = h_l(s_{lt}), \forall t \in \mathcal{T}$, which are gathered in a time series $\boldsymbol{\pi}_l = (\pi_{l1}, \ldots, \pi_{lT})^\top \in [0, 1]^T$. The instantaneous power output of each location $l \in \mathcal{L}$ is then computed by multiplying each entry in the normalized power output time series $\boldsymbol{\pi}_l$ by the technical potential $\bar{\kappa}_l$ and stored in a time series $\mathbf{p}_l = (p_{l1}, \ldots, p_{lT})^\top \in \mathbb{R}_+^T$.

Regions and buses: Furthermore, the set of locations $\mathcal{L}$ is partitioned into a collection of disjoint regions $\mathcal{L}_n \subseteq \mathcal{L}, \forall n \in \mathcal{N}_B$, where $\mathcal{N}_B, |\mathcal{N}_B| = B$, denotes the set of B electrical buses in the power system and $\mathcal{L}_n$ represents a set of candidate RES sites that may be connected to bus $n \in \mathcal{N}_B$. Furthermore, for any given set of locations $L \subseteq \mathcal{L}$, let $L_n = L \cap \mathcal{L}_n$ denote the (possibly empty) subset of locations that would be connected to bus $n \in \mathcal{N}_B$. An electricity demand time series $\lambda_n = (\lambda_{n1}, \ldots, \lambda_{nT})^\top \in \mathbb{R}_+^T$ is also associated with each bus $n \in \mathcal{N}_B$ and the total electricity demand time series $\lambda = (\lambda_1, \ldots, \lambda_T)^\top \in \mathbb{R}_+^T$ is obtained by summing the time series of all buses.

8.2.2 Siting framework

8.2.2.1 Combinatorial optimization model

The renewable power generation asset siting problem is formulated as a combinatorial optimization problem that selects a pre-specified number of sites so as to optimize a given siting criterion. More formally, let $k \in \mathbb{N}$ be the number of sites to be selected and let $f_C : \mathcal{P}(\mathcal{L}) \to \mathbb{R}$ be a function evaluating the score of any subset of locations $L \subseteq \mathcal{L}$ based on a given siting criterion C (where $\mathcal{P}(\mathcal{L})$ denotes the set of all subsets of $\mathcal{L}$). Then, the asset siting problem consists in selecting a subset of locations $L^\star$ such that

$$L^\star \in \operatorname{argmin}\{f_C(L) | L \subseteq \mathcal{L}, |L| = k\} \tag{8.1}$$

8.2.2.2 Siting criteria

Since no universally-accepted definition of complementarity exists, no single siting criterion can be devised in order to identify sets of complementary locations. Hence, in this chapter, seven different siting criteria adapted from the literature are considered. The first criterion measures the combined electricity output of a set of sites (PROD), which should be maximized. Although this criterion does not measure complementarity between locations *per se*, it can serve as a useful benchmark. Then, the second criterion relies on the correlation between pairs of sites (CORR). The first and second criteria, therefore, neglect the electricity load. By contrast, the next five criteria explicitly take the electricity load into account. More precisely, several criteria make use of the residual demand, which quantifies the mismatch between electricity consumption and production at any point in time. Thus, the third and fourth criteria focus on the average (ARD) and the maximum residual demand (MRD), respectively, while the fifth and sixth criteria assess the average (AV) and the maximum residual demand variability (MV), respectively. Finally, the seventh criterion estimates the fraction of time periods during which most sites fail to supply a pre-specified share of the electricity demand (CRIT).

Electricity output: The combined electricity output of a set of sites $L \subseteq \mathcal{L}$ can be simply obtained by summing the electricity produced by all locations $l \in L$ over all time periods $t \in \mathcal{T}$. Unlike other objectives described in this section, the combined electricity output should be maximized. Hence, in order to fit into the present siting framework, a slightly different objective must be used. More precisely, since maximizing a given objective function f_C is equivalent to minimizing $-f_C$, the score associated with this siting criterion is computed as follows:

$$f_{\text{PROD}}(L) = -\sum_{t\in\mathcal{T}}\sum_{l\in L} p_{lt} \tag{8.2}$$

Correlation: Since correlation coefficients can only be computed for pairs of sites (e.g., the correlation between two random variables representing wind speeds or power outputs is straightforward to compute), the correlation score of a set of sites $L \subseteq \mathcal{L}$ is obtained by taking the sum of correlation coefficients $R_{ij} \in [-1, 1]$ associated with every pair of sites $(i, j) \in L \times L, i \neq j$,

$$f_{\text{CORR}}(L) = \frac{1}{2}\sum_{i\in L}\sum_{j\in L, j\neq i} R_{ij} \tag{8.3}$$

Average residual demand: The residual demand is positive if there is a shortage of electricity in the system, while it is equal to zero if there is a production surplus. Thus, given a set of locations $L \subseteq \mathcal{L}$ and time period $t \in \mathcal{T}$, the residual demand can simply

be expressed as:

$$r_t(L) = \max\left\{0, \lambda_t - \sum_{l \in L} p_{lt}\right\} \tag{8.4}$$

The average residual demand score (Musselman et al., 2018) can therefore be computed as follows:

$$f_{\mathrm{ARD}}(L) = \frac{1}{T} \sum_{t \in \mathcal{T}} r_t(L) \tag{8.5}$$

Maximum residual demand: Alternatively, a maximum residual demand score may be computed for any set of locations $L \subseteq \mathcal{L}$ (Wu et al., 2017),

$$f_{MRD}(L) = \max\{r_t(L) | t \in \mathcal{T}\} \tag{8.6}$$

Average variability: The variability that a set of sites $L \subseteq \mathcal{L}$ exhibits can be measured by the absolute change in residual demand between consecutive time periods (Musselman et al., 2018). The resulting average variability score can be computed as follows:

$$f_{AV}(L) = \frac{1}{T-1} \sum_{t \in \mathcal{T}, t \neq 1} |r_t(L) - r_{t-1}(L)| \tag{8.7}$$

Maximum variability: A different variability metric that better captures abrupt increases in residual demand may also be considered (Musselman et al., 2018). More specifically, this metric quantifies the maximum increase in residual demand between consecutive time periods:

$$f_{MV}(L) = \max\{r_t(L) - r_{t-1}(L) | t \in \mathcal{T}, t > 1\} \tag{8.8}$$

Criticality: The spatiotemporal complementarity that subsets of sites display may also be measured by the empirical probability that they experience so-called *critical events* (Berger et al., 2020). Such events typically correspond to situations where most sites simultaneously experience low electricity production levels relative to a pre-specified fraction of the electricity demand. More formally, for any time period $t \in \mathcal{T}$ and set of locations $L \subseteq \mathcal{L}$, the number of locations $l \in L$ that produce more than a fraction $\varsigma_l \in [0, 1]$ of the demand can be calculated as follows:

$$N(L, t) = \sum_{l \in L} \max\left\{0, I\left(p_{lt} \geq \varsigma_l \lambda_t\right)\right\} \tag{8.9}$$

where $I(p_{lt} \geq \varsigma_l \lambda_t)$ is equal to 1 if $p_{lt} \geq \varsigma_l \lambda_t$ and 0 otherwise. If the number of sites producing enough electricity at each time period should be at least equal to $c \in \mathbb{N}$ for the time period to be non-critical, the fraction of time periods for which this condition

is not satisfied can be computed as follows:

$$f_{CRIT}(L) = 1 - \frac{1}{T} \sum_{t \in \mathcal{T}} \max\{0, (N(L, t) \geq c)\} \tag{8.10}$$

Note that minimizing this objective function is equivalent to maximizing the fraction of time periods during which at least c locations produce enough electricity. In addition, this criterion can be loosely interpreted as a discrete version of the average residual demand criterion, with the additional requirement that electricity production must be distributed across a number of sites.

8.2.2.3 Solution methods

Combinatorial optimization problems that are closely related to the one discussed above are known to be both NP-hard and hard to approximate even if the objective function has special properties such as monotonicity and submodularity (Nemhauser et al., 1978; Svitkina and Fleischer, 2011). Hence, although a detailed analysis of the properties of each objective function described above is beyond the scope of this chapter, it seems unlikely that polynomial-time algorithms systematically returning optimal solutions exist for each objective (except for the PROD criterion, whose associated optimization problem is straightforward to decompose and solve). In addition, although exact methods such as branch-and-bound algorithms may still yield optimal solutions for certain problem instances, they often become ineffective as the size of the problem grows (Berger et al., 2021; Musselman et al., 2018). Thus, one usually has to settle for approximate solution methods that produce good (suboptimal) solutions in a reasonable amount of time.

In this chapter, greedy algorithms are used to solve variants of the siting problem. These algorithms are conceptually simple, have low computational complexity, and sometimes offer worst-case performance guarantees (e.g., for coverage problems, Hochbaum and Pathria, 1998). In this context, greedy algorithms proceed as follows. Starting from an empty set, a location $l \in \mathcal{L} \setminus L$ is added to the incumbent solution L in each iteration. In order to identify this location, all unselected locations are enumerated and a score is computed for each one of them. This score typically reflects the value of adding a location to the incumbent solution, which can be computed using a pre-specified function $\hat{f}_C$ (that may be the natural objective function of the problem at hand or an auxiliary objective function designed to improve the performance of the algorithm (Berger et al., 2021)). The location with the best score is then added to the incumbent solution. If there is no single best location, ties are broken at random (i.e., one of the best locations is selected at random and added to the incumbent solution). This procedure is repeated until k locations have been added. The pseudocode in Fig. 8.1 summarizes these ideas. The details of this algorithm can be found in (Berger et al., 2021).

Input $\mathcal{L}$, k, $\hat{f}_C$
  $L \leftarrow \emptyset$ ▷ initialize incumbent solution
  while $|L| < k$ **do**
    $\tilde{L} \leftarrow \arg\min_{l \in \mathcal{L} \setminus L} \hat{f}_C(L \cup \{l\})$ ▷ retrieve best locations
    $l \leftarrow$ one location sampled from $\tilde{L}$ uniformly at random ▷ break ties
    $L \leftarrow L \cup \{l\}$ ▷ update incumbent solution
  end while
Output $L, \hat{f}_C(L)$

Figure 8.1 Pseudocode describing the workings of greedy algorithms used to solve variants of the siting problem.

8.2.3 Capacity expansion planning framework

Once a set of RES sites $L \in \mathcal{L}$ has been selected using the siting framework of the previous section, their corresponding resource time series $\{\boldsymbol{\pi}_l\}_{l \in L}$ and technical potentials $\{\bar{\kappa}_l\}_{l \in L}$ are provided as input data to the CEP framework that evaluates the impact of the underlying siting strategy on the capacities and costs of technologies deployed in the power system. The formulation of the CEP problem used for this purpose is presented next. Table 8.1 summarizes the notation used throughout this section.

First, a set of working assumptions are introduced in order to derive the CEP framework:

- Investment decisions in generation, transmission and storage assets are made by a central planner who also operates the system, has perfect foresight and knowledge (i.e., knows all exogenous techno-economic parameters and future events impacting the system with certainty), and whose goal is to minimize total system cost over a finite time horizon.
- A static investment model is considered, wherein investment decisions are made at the beginning of the time horizon. New capacity deployments are immediately available and remain constant throughout the entire time horizon. Operational decisions, on the other hand, are made at regular intervals (e.g., on an hourly basis) throughout the time horizon considered. The investment and operational problems are solved concurrently.
- Investments in generation, transmission and storage capacity are continuous (as opposed to discrete investments).
- The capacity of each RES plant selected in the siting stage is assumed to be constant throughout the optimization horizon and equal to the technical potential of the associated site.
- The network is represented by a set of existing nodes, which represent an aggregation of real electrical buses, and a set of existing transmission corridors, which connect the aforementioned nodes and to which transmission capacity expansion is limited (i.e., no new transmission corridors can be constructed).
- Network flows are represented via a lossless transportation model.

Table 8.1 Capacity expansion planning framework nomenclature.

Notation	Description
Indices & sets	
$c, \mathcal{C}$	Line, set of transmission corridors, $\mathcal{C} \subset \mathcal{N}_B \times \mathcal{N}_B$
$\mathcal{C}_n^+, \mathcal{C}_n^-$	Set of inbound links into node $n \in \mathcal{N}_B$, with $\mathcal{C}_n^+ = \{c \in \mathcal{C} \mid c = (u, n), u \in \mathcal{N}_n^+\}$, where $\mathcal{N}_n^+ = \{u \in \mathcal{N}_B \mid (u, n) \in \mathcal{C}\}$ and set of outbound links from node n, with $\mathcal{C}_n^- = \{c \in \mathcal{C} \mid c = (n, v), v \in \mathcal{N}_n^-\}$, where $\mathcal{N}_n^- = \{v \in \mathcal{N}_B \mid (n, v) \in \mathcal{C}\}$
$g, \mathcal{G}$	Conventional generation technology index and associated set
l, L_n	Site and set of sites associated with bus n
$n, \mathcal{N}_B$	Bus and set of buses
$r, \mathcal{R}$	Renewable technology index and set of RES technologies
$s, \mathcal{S}$	Storage technology index and set of storage technologies
$t, \mathcal{T}$	Time index, set of time steps
Parameters	
$\underline{\sigma}_{ns}, \bar{\sigma}_{ns}$	Initial and maximum installable capacity of storage technology s at node n [GWh]
μ_s	Minimum storage level of technology s (fraction of installed capacity) [-]
$\eta_s^{SD}, \eta_s^D, \eta_s^C$	Self-discharge, discharge and charge efficiency of storage technology s [-]
φ_s	Fixed energy-to-power ratio of storage technology s [-]
$\underline{\kappa}_c, \bar{\kappa}_c$	Initial and maximum installable (power) capacity of transmission line c, respectively [GW]
$\bar{\kappa}_l$	Technical potential of site l [GW]
$\underline{\kappa}_{nm}, \bar{\kappa}_{nm}$	Initial and maximum installable (power) capacity of technology $m \in \{g, r, s\}$ at node n [GW]
λ_{nt}	Electricity demand at node n and time t [GW]
π_{lt}	Availability of RES technology at site l and time t [p.u.]
π_{nmt}	Availability of generation technology m at node n and time t [p.u.]
θ^{ens}	Economic penalty for demand curtailment [MEUR/GWh]
θ_f^x, θ_v^x	Fixed (FOM, expressed in MEUR/GW*year) and variable (VOM, expressed in MEUR/GWh) operation and maintenance cost of technology $m \in \{g, l, s, c\}$
ω_t	Weight of each operating condition t in the objective function and CO_2 emissions
ω_s	Weight of each operating condition t in the operation of storage units
ζ^m	Annualized investment cost of technology $m \in \{g, l, s, c\}$ [MEUR/GW]
Ψ^{CO2}	Yearly CO_2 budget [Mt]
$\nu_g^{CO_2}$	Specific CO_2 emissions of generation technology g [MtCO2/GWh]
η_g	Thermal efficiency of generation technology g [-]
Variables	
e_{nst}	State of charge (energy) of storage s at node n and time t [GWh]
K_c	Installed capacity of transmission line c [GW]

(*continued on next page*)

Table 8.1 Capacity expansion planning framework nomenclature—cont'd

Notation	Description
K_{nm}	Installed capacity (power) of technology $m \in \{g, s, r\}$ at bus n [GW]
p_{nmt}	Feed-in at node n from technology $m \in \{g, r\}$ at time t [GW]
p^C_{nst}, p^D_{nst}	Charge and discharge flow of storage technology s at bus n and time t [GW]
p_{ct}	Power flow over transmission line c at time t [GW]
p_{lt}	Feed-in of site l at time t [GW]
p^{ens}_{nt}	Unserved demand at bus n and time t [GW]
q^{CO2}_{ngt}	CO_2 emissions associated with generation technology g, at node n and time t [Mt]
S_{ns}	Rated energy storage capacity for technology s at node n [GWh]

- No unit commitment constraints are considered (e.g., start-up, shut-down, minimum up/down-times for conventional generation units). Furthermore, the full operating range of these plants (from zero to maximum capacity) is assumed stable, and their ramping rates are unbounded (i.e., units can ramp from minimum (resp. maximum) capacity to maximum (resp. minimum) capacity from one time period to the next).
- Neither outages nor failures of power plants and network components are considered.
- Capacity factors of renewable power plants, the (inelastic) electricity demand, investment, and operating costs of all technologies as well as their technical parameters are all exogenous.

Putting these assumptions to use, the CEP model then reads:

$$\min_{\mathbf{K},(\mathbf{p}_t)_{t\in\mathcal{T}}} \left[\sum_{\substack{n\in\mathcal{N}_B \\ j\in\mathcal{G}\cup\mathcal{R}\cup\mathcal{S}}} \left(\zeta^j + \theta^j_f\right) K_{nj} + \sum_{\substack{n\in\mathcal{N}_B \\ s\in\mathcal{S}}} \zeta^s S_{ns} + \sum_{c\in\mathcal{C}} \left(\zeta^c + \theta^c_f\right) K_c \right]$$
$$+ \sum_{t\in\mathcal{T}} \left[\sum_{\substack{n\in\mathcal{N}_B \\ l\in L_n}} \theta^l_v p_{lt} + \sum_{\substack{n\in\mathcal{N}_B \\ m\in\mathcal{G}\cup\mathcal{R}}} \theta^g_v p_{nmt} + \sum_{\substack{n\in\mathcal{N}_B \\ s\in\mathcal{S}}} \theta^s_v \left(p^C_{\text{nst}} + p^D_{\text{nst}}\right) + \sum_{c\in\mathcal{C}} \theta^c_v |p_{ct}| + \sum_{n\in\mathcal{N}_B} \theta^{ens} p^{ens}_{nt} \right]. \tag{8.11}$$

$$\sum_{l\in L_n} p_{lt} + \sum_{g\in\mathcal{G}\cup\mathcal{R}} p_{\text{ngt}} + \sum_{s\in\mathcal{S}} p^D_{\text{nst}} + \sum_{c\in\mathcal{C}^+_n} p_{ct} + p^{\text{ens}}_{nt} = \lambda_{nt} + \sum_{s\in\mathcal{S}} p^C_{nst} + \sum_{c\in\mathcal{C}^-_n} p_{ct} \ , \quad \forall n \in \mathcal{N}_B \ , \quad \forall t \in \mathcal{T} \tag{8.12}$$

$$p_{lt} \le \pi_{lt} \bar{\kappa}_l \ , \quad \forall n \in \mathcal{N}_B \ , \quad \forall l \in \ L_n \ , \quad \forall t \in \mathcal{T} \tag{8.13}$$

$$p_{nmt} \le \pi_{nmt} \left(\underline{\kappa}_{nm} + K_{nm} \right), \quad \forall n \in \mathcal{N}_B \ , \quad \forall m \in \mathcal{G}\cup\mathcal{R}, \quad \forall t \in \mathcal{T} \tag{8.14}$$

$$\underline{\kappa}_{nm} + K_{nm} \leq \bar{\kappa}_{nm}, \quad \forall n \in \mathcal{N}_B, \quad \forall m \in \mathcal{G} \cup \mathcal{R} \tag{8.15}$$

$$q_{ngt}^{CO_2} = \nu_g^{CO_2} p_{ngt}/\eta_g, \quad \forall n \in \mathcal{N}_B, \quad \forall g \in \mathcal{G}, \quad \forall t \in \mathcal{T} \tag{8.16}$$

$$K_{ns} = \phi_s^{-1} S_{ns}, \quad \forall n \in \mathcal{N}_B, \quad \forall s \in \mathcal{S} \tag{8.17}$$

$$p_{\text{nst}}^{C/D} \leq \underline{\kappa}_{ns} + K_{ns}, \quad \forall n \in \mathcal{N}_B, \quad \forall s \in \mathcal{S}, \quad \forall t \in \mathcal{T} \tag{8.18}$$

$$\mu_s\left(\underline{\sigma}_{ns} + S_{ns}\right) \leq e_{\text{nst}} \leq \underline{\sigma}_{ns} + S_{ns}, \quad \forall n \in \mathcal{N}_B, \quad \forall s \in \mathcal{S}, \quad \forall t \in \mathcal{T} \tag{8.19}$$

$$e_{\text{nst}} = \eta_s^{SD} e_{\text{nst}-1} + \eta_s^C p_{\text{nst}}^C - p_{\text{nst}}^D/\eta_s^D, \quad \forall n \in \mathcal{N}_B, \quad \forall s \in \mathcal{S}, \quad \forall t \in \mathcal{T} \tag{8.20}$$

$$\underline{\sigma}_{ns} + S_{ns} \leq \bar{\sigma}_{ns}, \quad \forall n \in \mathcal{N}_B, \quad \forall s \in \mathcal{S} \tag{8.21}$$

$$\left|p_{ct}\right| \leq \underline{\kappa}_c + K_c, \quad \forall c \in \mathcal{C}, \quad \forall t \in \mathcal{T} \tag{8.22}$$

$$\sum_{\substack{n \in \mathcal{N}_B \\ g \in \mathcal{G} \\ t \in \mathcal{T}}} q_{ngt}^{CO2} \leq \Psi^{CO2} \tag{8.23}$$

The CEP problem described in Eqs. (8.11)–(8.23) is cast as a linear program whose objective function, shown in Eq. (8.11), includes the capacity-dependent upfront costs of additional generation, storage, and transmission assets required to supply pre-defined levels of electricity demand at each bus, as well as the fixed and variable operation and maintenance (O&M) costs associated with both existing and additional capacities for the three classes of assets mentioned previously. The loss of load is also penalized through a slack variable (featured in the energy balance constraint in Eq. (8.12)) that maintains problem feasibility when the supply from generation and storage assets or flows from transmission links is not sufficient to cover the electricity demand in full.

The operation of RES sites identified by the siting framework is constrained by Eq. (8.13). In this chapter, it is assumed that the sites identified via the siting framework are exploited at their full technical potential, thus no sizing variable is used to model these units. The next three equations model the operation and sizing of the remaining generation units, including RES technologies that are not sited. First, electricity generation from such units is constrained by their installed capacity via Eq. (8.14). Then, their installed capacity is bounded from above, as can be seen in Eq. (8.15). Finally, Eq. (8.16) expresses the volume of CO_2 emitted by dispatchable units running on fossil fuels in terms of their power output, thermal efficiency, and the specific emission levels of the underlying fuel. It is worth mentioning the two most common situations in which

Eqs. (8.14)–(8.16) are enforced. On the one hand, if dispatchable units are modeled (e.g., gas-fired power plants), the time-dependent availability π_{nt} in Eq. (8.14) is set to one across the entire optimization horizon. On the other hand, for RES technologies that are not sited via the siting framework (i.e., the ones included in $\mathcal{R}$), the aforementioned parameter is instantiated with a per-unit capacity factor time series that is aggregated at the spatial resolution represented by bus $n \in \mathcal{N}_B$.

Then, the sizing and operation of storage units is modeled via Eqs. (8.17)–(8.21). The energy-to-power ratio of new installations is enforced via an exogeneous parameter in Eq. (8.17). Constraint Eq. (8.18) bounds the charge and discharge rates of such installations (which are assumed symmetric) by their power rating. Furthermore, the state of charge of storage assets is, at each node and time step, bounded by minimum and maximum storage levels Eq. (8.19), while its dynamics are defined via Eq. (8.20). Finally, as for generation technologies, the installed capacity of storage assets can be bounded at each node by a maximum installable capacity, as seen in Eq. (8.21). The physics of power flows are represented by a simplified lossless transportation model expressed in Eq. (8.21), which limits the active power flows in transmission links to the corresponding transport capacities. Finally, constraint Eq. (8.22) enforces that system-wide CO_2 emissions remain below a pre-specified budget.

8.2.4 Implementation

The two-stage approach was implemented in Python 3.7 and Julia 1.4 (Bezanson et al., 2017). More precisely, the siting heuristics were implemented in the Julia programming language, while the data pre- and post-processing as well as the entire CEP routine, which relies on PyPSA 0.17 (Brown et al., 2018), was implemented in Python. The CEP model was solved with Gurobi 9.1. Simulations were performed on a workstation running under CentOS, with an 18-core Intel Xeon Gold 6140 CPU clocking at 2.3 GHz and 256 GB RAM. The code used in this chapter is available at (Radu et al., 2021) (siting framework) and (Dubois et al., 2021) (CEP framework), along with all relevant input data (e.g., resource and demand time series as well as all techno-economic assumptions) (Radu et al., 2021).

8.3 Case study

In this section, the case study used to investigate the impact of different onshore wind siting schemes on the design of the European power system is described. First, the data used to construct instances of the onshore wind siting problem are discussed. Then, the data used to instantiate the CEP framework introduced in the previous section are described.

First, three years (2017–2019) of hourly-sampled resource data (wind speed) with a spatial resolution of 0.25° in both coordinate directions were retrieved from the ERA5

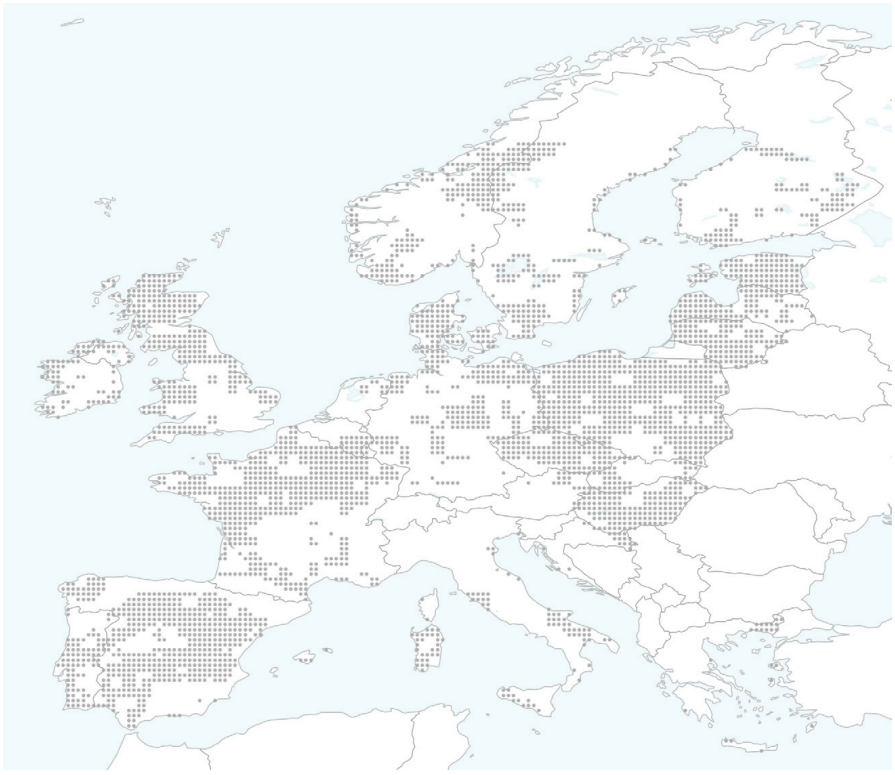

Figure 8.2 Candidate sites for onshore wind deployment across Europe (i.e., dark grey markers).

reanalysis database (European Centre for Medium-Range Weather Forecasts - ECMWF, 2020). Then, the mapping of resource data to capacity factor time series was done via transfer functions representing wind turbine models currently in production, namely two Vestas (the V164 and V90) and two Enercon (the E103 and E126) models. These models are suitable for different wind regimes and the specific transfer function used for each individual site was selected based on its underlying wind resource quality and its associated IEC wind class (International Electrotechnical Commission, 2019). In addition, a preprocessing step filtering reanalysis data grid points located within European geographical boundaries was performed in order to discard candidate sites where the installation of wind turbines would be impractical. First, all sites with a 5-year average wind speed below 4 *m/s* were discarded. Then, candidate sites where the population density is above 200 inhabitants per square kilometer were removed. Next, sites with an average terrain slope above 3% or with a forestry cover above 80% were also discarded. Finally, candidate locations found at latitudes greater than the 65th parallel were also discarded. Applying these filters leads to a total of 3609 candidate sites within European borders, which can be visualized in Fig. 8.2.

A report published by WindEurope in 2017 (Nghiem and Pineda, 2017) was used to build instances of the onshore wind siting problem. The central scenario of this study

envisions the operation of 263 GW of onshore wind power plants in 28 European countries by 2030. Since the renewable power generation asset siting problem is formulated as a combinatorial optimization problem that selects a pre-specified number of sites so as to minimize a given siting criterion, a function converting country-specific onshore capacities (κ, in GW) into a number of locations (k) is needed. This mapping (i.e., Eq. (8.24), where x denotes the ceiling function) requires two assumptions: i) the surface area of a representative grid cell (α_{cell}, i.e., the equidistant area surrounding a reanalysis dataset point, expressed in km^2) and ii) the power density of the underlying electricity generation technology (ρ_p, expressed in MW/km^2). In this chapter, a cell surface area of 521 km^2 (the surface area of a 0.25° by 0.25° square at 47.5° latitude) and an onshore wind power density of 2.4 MW/km^2 were considered. Used together in Eq. (8.24), these assumptions imply the deployment of $k = 211$ sites to host 263 GW of onshore wind power plants across Europe.

$$k = \kappa / \left(\rho_p \times \alpha_{\text{cell}}\right) \tag{8.24}$$

The Europe-wide demand time series $\lambda = (\lambda_1, \ldots, \lambda_T)^\top$ required in five of the seven siting formulations is retrieved from the Open Power System Data (OPSD) platform. Recall that in Eq. (8.9), a location $l \in \mathcal{L}$ is considered non-critical during time period $t \in \mathcal{T}$ if its generation potential exceeds a pre-defined share ς of the system-wide electricity demand. This share is assumed to be constant across the optimization horizon and equal to 23%, as suggested by Nghiem and Pineda (2017). Furthermore, the value of c in Eq. (8.10) is set such that the ratio between c and the number of deployments k is equal to 0.25 (i.e., at least 25% of all selected locations must produce enough electricity for a time period not to be critical).

The network topology used in the CEP framework is drawn from the 2018 version of the European Ten-Year Network Development Plan (TYNDP) (ENTSO-E, 2018). More specifically, the set $\mathcal{N}_B$ comprises 28 buses, each representing one country in the ENTSO-E region. It is assumed that all interconnections crossing bodies of water are developed as DC cables[2], while the remainder is AC lines. Furthermore, investments in transmission capacity are limited to the reinforcement of corridors already existing in the TYNDP "Reference Grid 2027" scenario, while the addition of new transmission corridors is not taken into account. The topology considered in this study is depicted in Fig. 8.3. Electricity demand time series $\{\lambda_n\}_{n \in \mathcal{N}_B}$ spanning the same years as the ones used in the siting stage (i.e., 2017–2019) are used in the CEP problem.

As previously mentioned, the optimal siting of onshore wind farms only is performed in the current exercise. In practical terms, this translates into the siting stage providing the sizing framework k different onshore wind profiles across Europe. By contrast, the

[2] These assumptions also apply for the France–Spain interconnector which, even though looking as if it cut straight through the land border, is expected to be developed through the Biscay Bay.

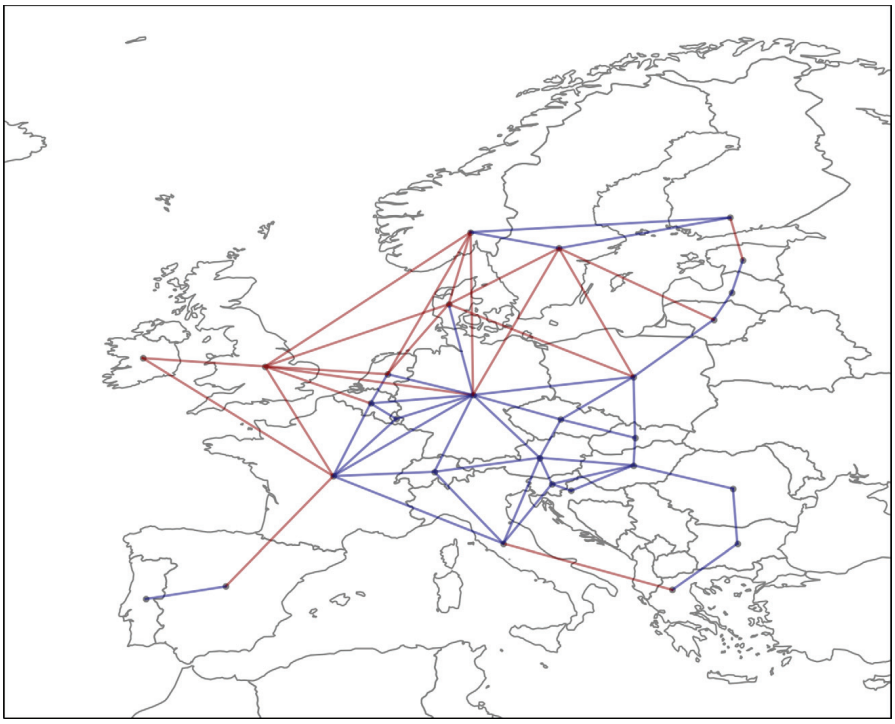

Figure 8.3 Network topology used in the proposed case study. Blue lines depict high-voltage alternating current (*HVAC*) cross-border interconnections, while red links represent high voltage direct current (*HVDC*) cross-border interconnections, according to the 2018 version of the TYNDP.

rest of the three available RES technologies (offshore wind, utility-scale, and distributed PV) are modeled via country-aggregated capacity factor time series retrieved from the *renewables.ninja* platform (Staffell and Pfenninger, 2016; Pfenninger and Staffell, 2016)[3]. Besides the four renewable resource-based electricity generation technologies, four others are available for electricity generation in the CEP problem, that is, combined-cycle gas turbines (CCGT), nuclear, as well as run-of-river and reservoir-based hydropower plants. All these technologies but onshore wind (whose site-specific capacity is not optimized and is assumed to be the technical potential of the locations selected in the siting stage), hydro and nuclear plants are sized in the CEP framework, and their technical potential provides an upper bound on the maximum capacity that may be deployed. In addition, all generation technologies but CCGT units are assumed to have non-zero installed capacities at the beginning of the optimization horizon[4]. The technical

[3] Moreover, note that solar PV generation profiles do not depend on the underlying technology (e.g., utility-scale or distributed PV profiles are identical for a given bus).

[4] Recall that the site-specific onshore wind capacities are assumed to be the technical potentials of the locations selected in the siting stage, thus one can interpret these values as existing capacity at the beginning of the optimization horizon. Offshore wind legacy capacity is obtained from *The Wind Power* database

potential of all sized RES technologies has been retrieved from the ENSPRESO database (Joint Research Centre, 2019), which provides technical potential estimates based on pre-defined scenarios modeling techno-economic and social restrictions associated with wind- and solar-based technologies. In the current exercise, low restriction scenarios were assumed for offshore wind and distributed PV installations. For the former, the resulting potential is estimated at 2065 GW[5]. With respect to the latter, roughly 1200 GW are available as technical potential across the continent[6]. For utility-scale solar PV, considering a high-restriction scenario yields a EU-wide technical potential of roughly 546 GW[7]. Lastly, the technical potential of the remaining generation technology to be sized in the CEP framework (i.e., CCGT) is assumed unconstrained.

Two technologies are available for storing electricity, namely pumped-hydro (PHS) and battery storage (Li-Ion) plants. The latter technology is modeled as a 4-hour duration storage unit (no independent sizing of power and energy ratings) with no legacy capacities across Europe. PHS units are not sized within the CEP framework at hand and the power ratings of existing plants are retrieved from European Commission - Joint Research Centre, Hydro Power Plant Database (2020), where a total of 54.5 GW/1950 GWh are reported. Finally, an EU-wide CO_2 budget is enforced and its value represents a 90% reduction in carbon dioxide emissions relative to 1990 levels (i.e., a CO_2 budget of 137.4 Mt per annum is considered).

8.4 Results

Simulation results generated with the siting and CEP frameworks are discussed in this section.

(Pierrot, 2020), which provides technical information for 99 GW of such units across European Seas and in different development stages (planned, approved, under construction, and operational). Utility-scale solar PV capacity data are retrieved from the *Wiki Solar* database (Wolfe, 2020) containing projects summing to over 46 GW throughout Europe and, as for offshore wind, in different development stages (planned, approved, under construction, and operational). Country-aggregated capacities for distributed PV are retrieved from the *SolarPowerEurope* market study (Beauvais et al., 2019), which reports the existence of 77 GW of such installations within European boundaries. Moreover, 61.5 GW of nuclear power capacity, 33.5 GW of run-of-river hydro power capacity, and 98.1 GW of reservoir-based hydro power capacity are available throughout the selected European countries (European Commission, 2020).

[5] Considering a low-restriction scenario, in which deployments are possible in inland waters (i.e., distances to shore between 0 and 120 nautical miles) and in depths of up to 1000 meters.

[6] According to a low-restriction development scenario that assumes a power density of 170 W/m^2 and a utilization share of the associated surfaces (e.g., flat roofs, inclined roofs, facades) varying from 6% to 70% depending on the orientation and the type of building.

[7] Assuming a similar high-restriction scenario that considers a power density of 85 W/m^2, 5% land utilization potential in high-irradiation areas, and no possibility of deploying utility-scale installations in areas with an average DNI below 1800 kWh/m^2 per year.

8.4.1 Siting outcomes

The sets of locations associated with the seven siting strategies are depicted in Fig. 8.4, where red markers indicate the geographical locations of renewable power generation sites selected for deployment. In the first subplot (top left), it can be seen that most of the 211 onshore wind sites selected by the scheme minimizing the average residual demand (ARD) are located along the coasts of the Atlantic Ocean, the North Sea, and the Baltic Sea. This suggests that wind power production patterns in these areas match aggregate European electricity demand patterns fairly well. The next subplot (top right) shows that most sites selected by the scheme minimizing the average residual demand variability (AV) are located in the British Isles and Scandinavia, with the remainder fairly evenly spread across Continental Europe, from the Iberian Peninsula to the Baltics. Then, the third subplot (second row, left) indicates that the siting strategy minimizing the correlation between sites (CORR) distributes clusters of onshore wind sites across European regions known to have distinct wind regimes (incl. Scandinavia, the British Isles, the Iberian Peninsula and the Eastern Mediterranean region) (Grams et al., 2017). The fourth subplot (second row, right) shows that a high proportion of the total number of sites selected by the siting strategy minimizing the empirical probability of observing so-called critical events (CRIT) are located in the British Isles and South-West Europe (i.e., France and Iberia). Many sites are also deployed in the Jutland Peninsula. These observations are consistent with earlier findings suggesting that these wind production patterns match aggregate European electricity demand patterns well. Note that more than a dozen sites are also deployed in areas with wind regimes distinct from the ones typically found in Northern and Western Europe (e.g., the Eastern Mediterranean or the Baltic region). The fifth subplot (third row, left) shows that the scheme minimizing the maximum residual demand (MRD) spreads most onshore wind sites along European coastlines from Estonia to Denmark and Norway, in the British Isles, around the Iberian Peninsula, in Italy, and in Greece. In addition, some inland wind regimes are also harnessed by this scheme. More specifically, sites are selected in areas swept by the Mistral and Tramontane in France (Obermann et al., 2018), as well as the Cierzo in Spain (Gonzalez et al., 2018). In the sixth subplot (third row, right), it can be seen that the siting strategy seeking to minimize the maximum residual demand variability (MV) results in the vast majority of onshore sites being deployed inland, unlike previous siting criteria. Sites are also spread relatively evenly across Europe. Finally, it can be seen in the last subplot (bottom left) that the set of locations maximizing electricity output (PROD) happen to exactly coincide with the set of locations minimizing the average residual demand (ARD) over the time horizon considered. This observation suggests that at the European level, simply deploying renewable power plants at the most productive locations may be sufficient to achieve a degree of complementarity between them equivalent to that obtained with a siting criterion specifically designed to identify locations whose regimes

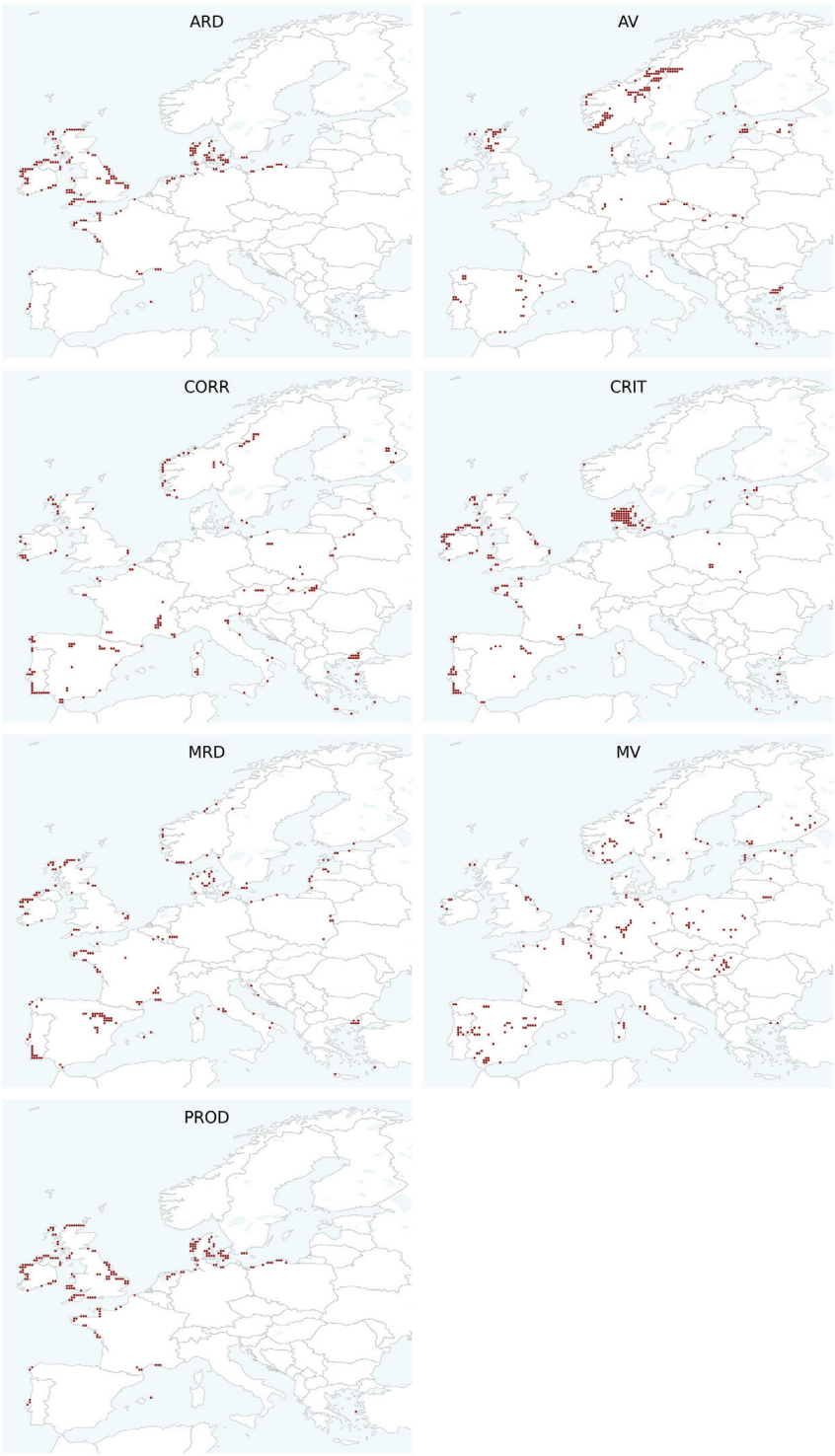

Figure 8.4 Set of locations selected using each of the seven siting strategies. In these plots, the selected locations are shown as dark red markers.

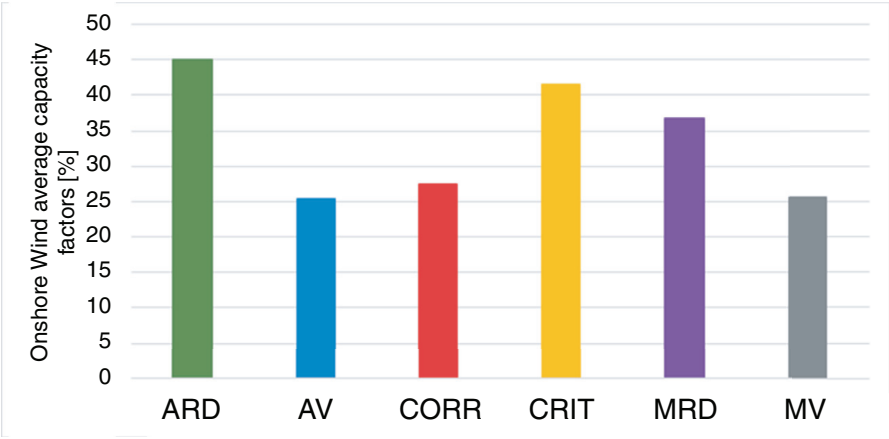

Figure 8.5 Average capacity factors of onshore wind sites for the ARD, AV, CORR, CRIT, MRD, and MV schemes, respectively.

are complementary (in the sense of the average residual demand). Since the PROD siting criterion yields the exact same locations as the ARD criterion, describing results pertaining to the latter suffices and the former is omitted in the following.

Fig. 8.5 gathers the average capacity factor of onshore wind installations for each siting scheme, which was computed by averaging capacity factor time series in space and time. The ARD criterion is the one yielding the set of locations whose average capacity factor is the highest (around 45%), followed by the CRIT (around 41%) and MRD (approximately 37%) criteria. Note that all of these criteria achieve average capacity factors that are higher than 35%. By contrast, all other criteria lead to average capacity factors that are only slightly above 25%. Hence, since all locations roughly have the same technical potential, the theoretical power generation potential of sets of locations identified with the AV, CORR, and MV criteria is much lower. This observation can be explained as follows. Roughly speaking, the lower the absolute residual electricity demand over time, the better the ARD, CRIT, and MRD scores. Although sites that are very productive may not always lead to low residual demand levels (e.g., if they all share the same power generation profile that happens to be very different from the electricity demand profile), sites that produce little electricity will almost certainly result in high residual demand levels. Moreover, even though the AV and MV criteria take the residual demand into account, they only measure its variation. Hence, sites with aggregate production profiles that are all translated upwards or downwards would essentially yield the same scores. Finally, since the CORR score (which is based on the Pearson correlation coefficient) is normalized, the absolute production level does not matter.

The statistical distribution of the Europe-wide (aggregate) residual demand associated with each siting strategy is shown in Fig. 8.6. In order to generate this plot, the aggregate

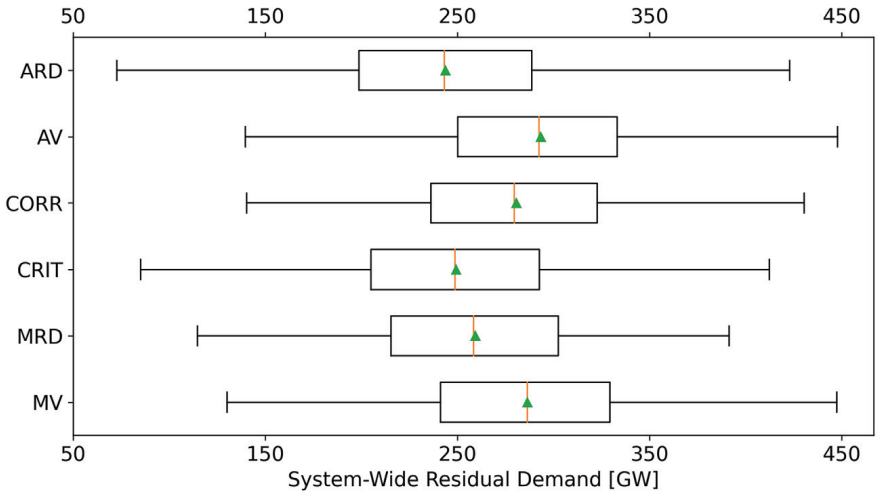

Figure 8.6 Box plots of Europe-wide residual demand for the siting strategies considered. Orange lines represent median values, whereas green triangles represent mean values.

onshore wind production time series was computed by summing the production time series of all 211 sites. Each production time series was computed by multiplying the capacity factor time series of the corresponding location by its capacity, which was assumed equal to its technical potential. Then, the aggregate residual demand signal was calculated by subtracting the aggregate onshore wind time series from the Europe-wide aggregate demand time series. In the box plots below, the orange lines and green triangles represent the median and mean, respectively, while the box itself spans the interquartile range (i.e., the range between the first and third quartiles). Several observations can be made. First, as expected, the ARD scheme has the lowest average residual demand (i.e., it has the leftmost green arrow, which is around 245 GW). The CRIT scheme has the second-lowest average residual demand (approximately 250 GW), which confirms the intuition that this criterion can loosely be interpreted as a discrete version of the ARD criterion. The MRD strategy then comes third (roughly 255 GW), followed by the CORR scheme (around 275 GW). The two schemes with the highest average residual demand are MV (about 290 GW) and AV (approximately 295 GW). Second, the MRD scheme has the lowest maximum residual demand (roughly 415 GW), which is consistent with the definition of this criterion. The CRIT scheme comes second (around 425 GW), followed by the ARD scheme (roughly 435 GW). The CORR criterion comes fourth (approximately 440 GW), while the AV and MV schemes perform equally badly in terms of maximum residual demand (about 450 GW each). Finally, minimum residual demand levels roughly fall between 75 and 145 GW, which implies that onshore wind power plants alone cannot generate any production surplus.

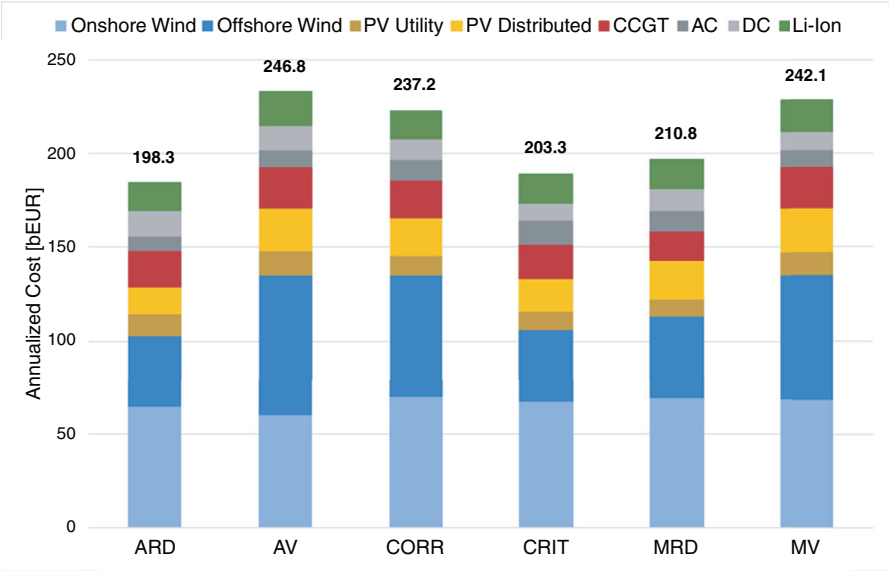

Figure 8.7 Total annualized system cost broken down by technology for each siting criterion. Each segment of a bar represents the sum of (1) capital expenses associated with the deployment of additional capacity for technologies that are sized and (2) O&M costs taking into account the total installed capacity of each considered technology. The figures on top of each bar represent the total system cost of the corresponding siting scheme, where all capital expenditure associated with legacy plants was neglected.

8.4.2 Impact of siting strategies on system design and economics

Fig. 8.7 displays the breakdown of the annualized system cost by technology for each siting strategy. The cheapest system configuration is obtained with the ARD siting scheme. Since the ARD and PROD schemes provide identical sets of locations (see Fig. 8.4), this also implies that selecting the most productive onshore wind locations results in the cheapest power system design. The CRIT scheme leads to a system configuration that is roughly 2.5% more expensive, while using the MRD criterion results in a system design that is about 5% more expensive. All other schemes lead to configurations that are (roughly) 20% to 25% more expensive. It is worth noting that RES technologies account for most of the annualized system cost (well over 60% in most cases), the vast majority of which is in the form of CAPEX. Among RES technologies, wind power plants (both onshore and offshore) make up the largest share of costs (over 75%). The remaining share of total system cost is fairly evenly split between gas-fired power plants, batteries, and transmission assets (when the costs of both AC and DC lines are summed). Differences in total system cost between schemes mostly stem from the amount of money spent on offshore wind power plants. Indeed, offshore wind costs reported for the three cheapest schemes (ARD, CRIT, and MRD) are much smaller than those observed for the three

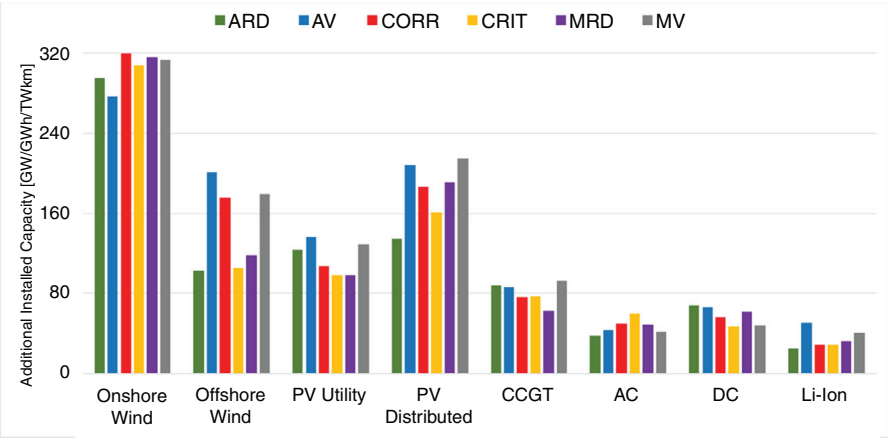

Figure 8.8 Additional capacities (i.e., legacy capacities are not accounted for) of each technology identified by the CEP framework (except onshore wind power plants) for each siting strategy. Capacities of generation, storage and transmission technologies are expressed in GW, GWh, and TWkm, respectively. A summary of existing legacy capacities is provided in the Case Study description.

other schemes (MV, AV, and CORR). Costs stemming from gas-fired power plants are also smaller for the MRD and CRIT schemes, although this has a limited impact on total system cost. Finally, although the share of costs stemming from transmission assets remains fairly constant across schemes, the breakdown by transmission technology (i.e., AC vs DC) tends to change.

Fig. 8.8 gathers the additional installed capacities for the eight technologies sized in the CEP problems while Fig. 8.9 displays the average annual electricity generation (in TWh) broken down by technology for each siting strategy. Recall that onshore wind capacities were computed based on the technical potential of locations identified in the siting stage and were therefore not sized in the CEP model. Onshore wind capacities vary (roughly) between 275 GW (for the MV scheme) and 320 GW (for the CORR scheme). Since different schemes have very different average capacity factors (see Fig. 8.5), the amounts of electricity produced by onshore wind power plants also differ very widely between schemes, as shown in Fig. 8.9. This essentially drives the deployment of offshore wind power plants, which make up for any deficit in onshore wind electricity production. This intuition is confirmed by the fact that the combined share of electricity produced by onshore and offshore wind power plants remains roughly constant across siting strategies, as shown in Fig. 8.9. Since the cost of offshore wind power plants is much higher than that of other renewable power generation technologies, this observation largely explains the cost differences observed between different schemes. On the other hand, no obvious trend in the deployment of solar PV capacity can be seen in Fig. 8.8. The deployment of battery storage systems, however, seems to be directly correlated to the amount of solar PV capacity in the system. It is worth noting that the MRD scheme is the one for

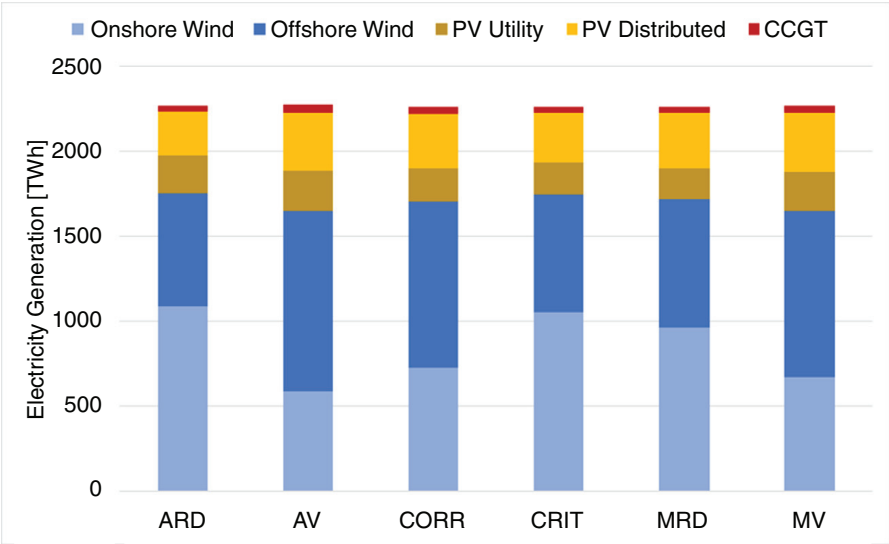

Figure 8.9 Average annual power generation (in TWh) broken down by technology for each siting strategy.

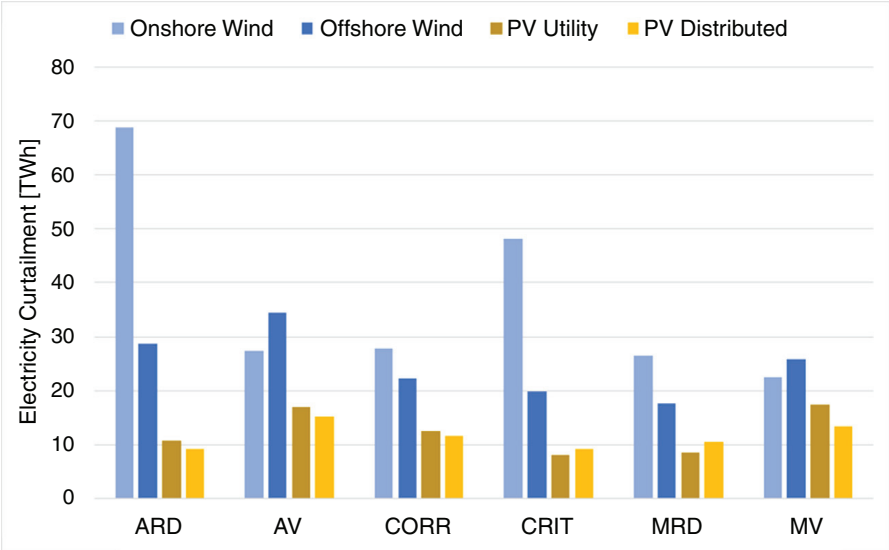

Figure 8.10 Average annual curtailment (TWh) broken down by renewable power generation technology.

which the capacity of gas-fired power plants is the lowest. This observation is consistent with the fact that this scheme is also the one with the lowest maximum residual demand. However, the amount of electricity produced by gas-fired power plants remains fairly constant across schemes and represents a very small fraction of the total (no more than a few percentage points).

Finally, Fig. 8.10 shows the average annual amount of curtailment broken down by renewable power generation technology for each siting strategy. The siting strategies with the highest average capacity factors (namely ARD and CRIT) are also the ones for which the amount of onshore wind electricity curtailment is the highest. On the other hand, the MV and AV schemes are the ones for which the amount of solar PV electricity curtailment is the highest.

8.5 Conclusion

This chapter analyses the role that complementarity may play in renewable power generation asset siting decisions and its impact on power system design and economics. To this end, a two-stage approach is employed. In the first stage, a siting method is used to select a prespecified number of sites optimizing a pre-defined siting criterion. In the second stage, the set of sites identified in the first stage is passed to a joint generation-transmission-storage CEP model, which identifies the optimal power system configuration. The code implementing the method is also made available to the community.

Seven different siting criteria adapted from the literature are analyzed in a case study focusing on the deployment of onshore wind power plants in the European power system. More precisely, roughly 200 onshore wind locations were selected (out of more than 3000) so as to optimize each siting criterion and passed to a CEP model. Interestingly, the set of locations selected by the scheme that minimizes the average residual demand was found to coincide with that of the scheme maximizing the electricity output, suggesting that selecting onshore wind locations in the most productive European regions could suffice to obtain sets of locations that display a high degree of complementarity. In addition, the cheapest system design was obtained with these schemes, while the schemes minimizing the variability of the residual demand and the correlation between wind regimes were between 20% and 25% more expensive. This outcome can be largely attributed to the fact that the latter schemes have much higher residual demand levels, which result in renewable electricity production deficits that must be compensated for by additional offshore wind capacity deployments.

In future work, several research directions can be envisaged. In the siting stage, extending the case study to include several types of renewable resources and technologies (e.g., solar PV, onshore, and offshore wind) would make it possible to gain a better understanding of their spatiotemporal complementarity and interactions. In addition, accounting for legacy units in the siting stage would enable a better estimation of where new RES assets should be deployed in order to maximize resource complementarity while accounting for generation patterns of existing renewable power plants. In the CEP stage, several improvements could be considered. First, increasing the spatial resolution of the network representation (i.e., from a one-node-per-country set-up to a representation based on the European territorial NUTS divisions, for instance) would provide a

better approximation of the need for technologies that are not included in the siting stage. Then, the model formulation could be updated to improve the representation of power flows (e.g., via a linearized version of the AC power flow equations), which becomes particularly relevant if a higher-resolution network topology is employed, as this would enable a more accurate estimation of power flow patterns and their impact on transmission sizing. Third, including unit commitment constraints and start-up costs for dispatchable power plants as well as system adequacy requirements (e.g., reserve requirements) in the CEP model would make it possible to better estimate system costs stemming from RES variability. Lastly, accounting for short-term renewable resource uncertainty would result in more realistic dispatch decisions and power system designs.

References

Berger, M., Radu, D., Fonteneau, R., Henry, R., Glavic, M., Fettweis, X., Le Du, M., Panciatici, P., Balea, L., Ernst, D., 2020. Critical time windows for renewable resource complementarity assessment. Energy 198. doi:10.1016/j.energy.2020.117308.

Berger, M., Radu, D., Dubois, A., Pandzic, H., Dvorkin, Y., Louveaux, Q., Ernst, D., 2021. Siting renewable power generation assets with combinatorial optimisation. Optim Lett. https://doi.org/10.1007/s11590-021-01795-0.

Beauvais, A., Herrero Cangas, M., Chevillard, N., Heisz, M., Labordena, M., Rossi, R., EU Market Outlook for Solar Power 2019-2023, Solar Power Europe, Tech. Rep., 2019. [Online]. Available: https://www.solarpowereurope.org/eu-market-outlook-for-solar-power-2019-2023/.

Bezanson, J., Edelman, A., Karpinski, S., Shah, V.B., 2017. Julia: a fresh approach to numerical computing. SIAM Rev. 59 (1), 65–98. https://doi.org/10.1137/141000671.

Brown, T., Horsch, J., Schlachtberger, D., 2018. PyPSA: python for power system analysis. J. Open Res. Soft. 6 (1). https://doi.org/10.5334/jors.188.

Dubois, A., Radu, D., Berger, M., 2021. Replan—a tool for expansion planning problems in energy systems. https://github.com/montefesp/replan/releases/tag/v0.0.5. (Accessed 25 June 2021).

Engeland, K., Borga, M., Creutin, J.-D., Francois, B., Ramos, M.-H., Vidal, J.-P., 2017. Space-time variability of climate variables and intermittent renewable electricity production—a review. Renew. Sustain. Energy Rev. 79. https://doi.org/10.1016/j.rser.2017.05.046.

ENTSO-E, 2018. Maps & data: TYNDP 2018. https://tyndp.entsoe.eu/maps-data. (Accessed 8 December 2021).

European Centre for Medium-Range Weather Forecasts - ECMWF, 2020. Copernicus knowledge base - ERA5 data documentation. https://confluence.ecmwf.int//display/CKB/. (Accessed 8 December 2021).

European Commission - Joint Research Centre, JRC Hydro-power plants database, 2020. [Online]. Available: https://github.com/energy-modelling-toolkit/hydro-power-database.

European Commission - Joint Research Centre, 2019. The Joint Research Centre Power Plant Database (JRC-PPDB). https://ec.europa.eu/jrc/en/publication/joint-research-centre-power-plant-database-jrc-ppdb. (Accessed 8 December 2021).

European Commission - Joint Research Centre, Hydro Power Plant Database, 2020. URL: https://github.com/energy-modelling-toolkit/hydro-power-database. (Accessed 8 December 2021).

Giebel, G., 2000. On the Benefits of Distributed Generation of Wind Energy in Europe. University of Oldenburg http://www.drgiebel.de/GGiebel_DistributedWindEnergyInEurope.pdf. (Accessed 8 December 2021).

Gonzalez, S., Callado, A., Werner, E., Escribà, P., Bech, J., 2018. Coastally trapped disturbances caused by the tramontane wind on the northwestern Mediterranean: numerical study and sensitivity to short-wave radiation. Q J R Meteorol. Soc. 144, 1321–1336. https://doi.org/10.1002/qj.3320.

Grams, C.M., Beerli, R., Pfenninger, S., Staffell, I., Wernli, H., 2017. Balancing Europe's wind-power output through spatial deployment informed by weather regimes. Nature Clim. Change 7, 557–562. https://doi.org/10.1038/nclimate3338.

Hochbaum, D.S., Pathria, A., 1998. Analysis of the greedy approach in problems of maximum k-coverage. Naval Res. Logist. 45 (6), 615–627. https://doi.org/10.1002/(SICI)1520-6750(199809)45:6<615::AID-NAV5>3.0.CO;2-5.

International Electrotechnical Commission, 2019. IEC 61400-1:2019: Wind energy generation systems—Part 1: Design requirements. https://webstore.iec.ch/publication/26423. (Accessed 8 December 2021).

Joint Research Centre, 2019. ENSPRESO—an open, EU-28 wide, transparent and coherent database of wind, solar and biomass energy potentials. https://data.jrc.ec.europa.eu/collection/id-00138. (Accessed 8 December 2021).

Jurasz, J., Canales, F.A., Kies, A., Guezgouz, M., Beluco, A., 2020. A review on the complementarity of renewable energy sources: concept, metrics, application and future research directions. Sol. Energy 195. https://doi.org/10.1016/j.solener.2019.11.087.

Milligan, M.R., Artig, R., 1999. Choosing wind power plant locations and sizes based on electric reliability measures using multiple-year wind speed measurements. In: U.S. Association for Energy Economics Annual Conference.

Musselman, A., Thomas, V.M., Boland, N., Nazzal, D., 2018. Optimizing wind farm siting to reduce power system impacts of wind variability. Wind Energy. https://doi.org/10.1002/we.2328.

Nemhauser, G.L., Wolsey, L.A., Fisher, M.L., 1978. An analysis of approximations for maximizing submodular set functions-I. Math. Program. 14, 265–294. https://doi.org/10.1007/BF01588971.

Nghiem, A., Pineda, I., 2017. Wind Energy in Europe: Scenarios for 2030. WindEurope P. Tardieu, Ed. https://windeurope.org/wp-content/uploads/files/about-wind/reports/Wind-energy-in-Europe-Scenarios-for-2030.pdf. (Accessed 8 December 2021).

Obermann, A., Bastin, S., Belamari, S., Conte, D., Gaertner, M.A., Li, L., Ahrens, B., 2018. Mistral and Tramontane wind speed and wind direction patterns in regional climate simulations. Climate Dyn. 51. https://doi.org/10.1007/s00382-016-3053-3.

Open Power System Data, 2019. Data package time series. https://data.open-power-system-data.org/time_series/2019-06-05. (Accessed 8 December 2021).

Pierrot, M., The Wind Power - Wind Energy Market Intelligence, 2020. [Online]. Available: https://www.thewindpower.net/store_continent_en.php?id_zone=1001.

Pfenninger, S., Staffell, I., 2016. Long-term patterns of European PV output using 30 years of validated hourly reanalysis and satellite data. Energy 114. https://doi.org/10.1016/j.energy.2016.08.060.

Radu, D., Berger, M., Dubois, A., 2021. Resite: a framework for RES siting leveraging resource complementarity. Available: https://github.com/dcradu/resite_ip/releases/tag/v0.0.2 (Accessed 13 January 2022).

Radu, D., Berger, M., Dubois, A., Fonteneau, R., Pandzic, H., Dvorkin, Y., Louveaux, Q., Ernst, D., 2022. Assessing the impact of offshore wind siting strategies on the design of the European power system. Applied Energy. https://doi.org/10.1016/j.apenergy.2021.117700.

Staffell, I., Pfenninger, S., 2016. Using bias-corrected reanalysis to simulate current and future wind power output. Energy 114. https://doi.org/10.1016/j.energy.2016.08.068.

Svitkina, Z., Fleischer, L., 2011. Submodular approximation: sampling-based algorithms and lower bounds. SIAM J. Comput. 40 (6), 1715–1737. https://doi.org/10.1137/100783352.

Wolfe, P. Wiki Solar - The authority on utility-scale solar power, 2020. [Online]. Available: https://www.wiki-solar.org/data/index.html.

Wu, G.C., Deshmukh, R., Ndhlukula, K., Radojicic, T., Reilly-Moman, J., Phadke, A., Kammen, D.M., Callaway, D.S., 2017. Strategic siting and regional grid interconnections key to low-carbon futures in African countries. Proc. Natl Acad. Sci. 114. https://doi.org/10.1073/pnas.1611845114.